Astron. Astrophys. 307, 703–707 (1996)

ASTRONOMY AND ASTROPHYSICS

Peak statistics on COBE maps

R. Fabbri[1] **and S. Torres**[2]

[1] Dipartimento di Fisica dell'Università, Sezione di Fisica Superiore, Via S. Marta 3, I-50139 Firenze, Italy
[2] Observatorio Astronómico Nacional, Universidad Nacional de Colombia, Bogotà, Colombia

Received 13 January 1995 / Accepted 1 August 1995

Abstract. We perform the stastistics of temperature maxima and minima in COBE-DMR 2-year maps. For power-law spectra the surface distribution of peaks implies an amplitude consistent with more conventional analyses of COBE data (for instance, we get $Q_{\rm rms-PS} = 17 \pm 3$ μK for a spectral index $n = 1$), but not with the measured quadrupole $Q_{\rm rms} = 6 \pm 3$ μK. This provides further support for the existence an infrared cutoff in the cosmic spectrum.

Key words: cosmic microwave background – cosmology: observations – methods: statistical

1. Introduction

The COBE experiment (Bennet et al. 1992, 1994; Smoot et al. 1992) has stimulated a considerable amount of work on cosmic structure. Current tests usually exploit the angular correlation function and several harmonic amplitudes of the sky temperature field (see e.g, Adams et al. 1992; Kashlinsky 1992; Efstathiou et al. 1992; Kofmann et al. 1993; Gorski et al. 1994). However, several more tests have been suggested over the years for a thorough investigation of the properties of the anisotropy field of the cosmic background radiation. These often involve the distribution and features of hot and cold spots, which can provide useful checks of the Gaussian nature of the fluctuations (Sazhin 1985; Bond & Efstathiou 1987; Coles & Barrow 1987; Coles 1988; Martínez-González & Sanz 1989; Gott et al. 1990). Measurable quantities include the number of spots $N_{\rm iso}$ defined by isotemperature contours, the spot boundary curvature or genus G, the spot excursion area, and so on. A first analysis of COBE-DMR maps along these lines has been performed by Torres (1994). A definition of spots independent of isotemperature contours considers local maxima and minima of temperature (Bond & Efstathiou 1987, Vittorio & Juszkiewicz 1987), and is thereby not connected to the topological features of spots. Differing from $N_{\rm iso}$, the dependence of the number of (positive and/or negative) peaks $N_{\rm peak}$ on threshold is not universal for Gaussian fields. This latter approach was adopted by Fabbri & Natale (1993, 1995) in studies of the 2-dimensional distribution of extragalactic IRAS sources, but has not yet been applied to the cosmic background radiation.

In this work we analyze the statistics of local maxima and minima in COBE-DMR 2-year maps. We found that in this kind of analysis the detector noise must be taken into account very carefully since $N_{\rm peak}$ is sensitive also to high order harmonics where noise dominates (cf. Fabbri 1992). However, due to a highly nonlinear dependence of $N_{\rm peak}$ on the harmonic strengths, the presence of structured signals in COBE maps reduces its value below the level measured in pure noise maps. (The identification of genuine peaks in the radiation temperature is not required at all in our analysis.) We find that the distributions of positive and negative peaks are mutually consistent, and the results from this statistics agree with those of earlier tests. Therefore, we find no evidence for non-Gaussian features in the fluctuations. More precisely, fitting Gaussian power-law models of cosmic structure to the peak distribution we recover a clear anticorrelation between the spectral index n and the predicted rms quadrupole $Q_{\rm rms-PS}$ (Seljak & Bertschinger 1993; Smoot et al. 1994): We get $Q_{\rm rms-PS} = 17 \pm 3$ μK for $n = 1$ and 14 ± 3 μK for $n = 1.5$, where the error bars include uncertainties deriving from the treatment of noise as well as cosmic variance. These numbers, altough they agree with previous evaluations of the quadrupole from higher order harmonics, are not consistent with its direct determination providing $Q_{\rm rms} = 6 \pm 3$ μK (Bennet et al. 1994). So the recently discovered discrepancy is confirmed by the properties of the peak distribution, which depend on the harmonic content of the angular distribution up to $\ell \sim 50$.

2. The peak number test

We analyzed the 2-year 53(A+B) DMR maps processed with a 2.9° smoothing (Wright et al. 1993) and dipole subtraction. Considering the Northern and Southern hemispheres separately, we constructed two pole-centered maps, each containing 12892 pixels, using the coordinate transformation $\theta_1 = 2 \sin\left[\frac{1}{2}\left(\frac{\pi}{2} - |b|\right)\right]$, $\phi_1 = l$, with b and l the Galactic coordinates. After masking low Galactic latitudes, $|b| < 20°$, we were

Send offprint requests to: R. Fabbri

Table 1. No-threshold peak numbers

Peak set	$(A+B)$ Maps $\|b\| > 20°$	$(A+B)$ Maps Extrapolated†	$(A-B)$ Maps No mask
Hot, North	50	76.6 ± 10.8	95
Cold, North	47	72.0 ± 10.5	99
Hot, South	48	73.6 ± 10.6	105
Cold, South	53	81.2 ± 11.2	97
Hot, total	98	150.2 ± 15.2	200
Cold, total	100	153.3 ± 15.3	196
Hot/Cold Average	99	151.7 ± 10.8	198

†To full sky or hemispheres, including masked regions

left with 8412 pixels per map. We then looked for temperature peaks using the algorithms of Fabbri & Natale (1993, 1995).

Table 1 gives the no-threshold numbers of peaks, both actually detected and extrapolated to the entire sky and to the North and South hemispheres (2nd and 3rd column, respectively). Figure 1 reports the extrapolated numbers vs. a threshold factor ν. This is the peak height normalized to the sky rms fluctuation $C^{\frac{1}{2}}(0)$; for cold spots, $N_{\rm peak}$ gives the number of minima below $-C^{\frac{1}{2}}(0)\nu$. For distributions of only positive *or* negative peaks the statistical errors at 1-sigma confidence levels are evaluated as $\left(N_{\rm peak}/f_{\rm U}\right)^{\frac{1}{2}}$, with $f_{\rm U} = 0.652$ the unmasked fraction of the sky. Within such error limits, we find no significant difference between the distributions of positive and negative peaks; this result provides support for the Gaussian nature of cosmic perturbations. In the figure we also report the full-sky average number of positive and negative peaks. This average will be compared with theoretical models below, because of the smaller (by a factor $\sqrt{2}$) relative error.

For the interpretation of the above data, we must consider that both cosmic signal and noise contribute to the temperature field $T(\theta,\phi) = \sum a_{\ell m} Y_{\ell m}(\theta,\phi)$. The expectation values of the numbers of local maxima and minima are determined by the variances $a_\ell^2 = \sum_m \langle \mid a_{\ell m} \mid^2 \rangle$. For a Gaussian field the full-sky $N_{\rm peak}$ is given by

$$\langle N_{\rm peak}(\nu)\rangle = \sqrt{\frac{2}{\pi}}\theta^{*-2}\left\{\gamma^{*2}\nu\exp\left(-\frac{1}{2}\nu^2\right)\right.$$
$$+\frac{\gamma^*\left(1-\gamma^{*2}\right)^{\frac{3}{2}}}{\sqrt{2\pi}}\exp\left(-u_2^2\nu^2\right)+\sqrt{\frac{\pi}{6}}\,\mathrm{erfc}\left(\sqrt{\frac{3}{2}}u_1\nu\right)$$
$$-\frac{1}{2}\int_\nu^\infty\left[\gamma^{*2}(y^2-1)\exp\left(-\frac{1}{2}y^2\right)\mathrm{erfc}\left(\gamma^*u_2y\right)\right.$$
$$\left.\left.+\,u_1\exp\left(-\frac{3}{2}u_1^2y^2\right)\mathrm{erfc}\left(\gamma^*u_1u_2y\right)\right]\mathrm{d}y\right\}, \qquad (1)$$

where

$$u_1 = \left(3-2\gamma^{*2}\right)^{-\frac{1}{2}}, \quad u_2 = \left[2\left(1-\gamma^{*2}\right)\right]^{-\frac{1}{2}}, \qquad (2)$$

and the properties of the anisotropy field are summarized by the parameters θ^* and γ^* (Bond & Efstathiou 1987; Fabbri 1992)

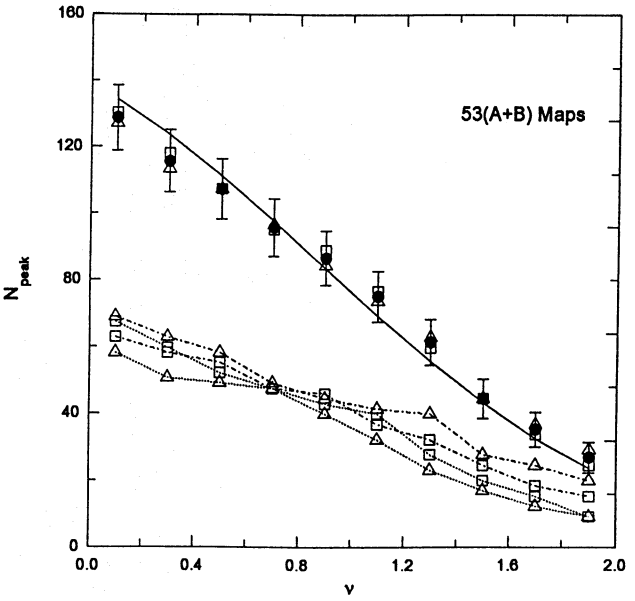

Fig. 1. The peak number $N_{\rm peak}$ vs. threshold in COBE-DMR maps. Open squares (triangles) denote positive (negative) peaks. The four lowest curves give the peak numbers extrapolated to the Northern (dotted lines) and Southern (dash-dotted) halves of the sky. The remaining curves refer to the full sky. Filled circles give the average numbers of positive and negative peaks. The full line describes a power-law model with $n = 1$ and $Q_{\rm rms-PS} = 18.5\ \mu$K, corresponding to the fit procedure S31 in Table 2

given by

$$\theta^{*2} = \left[2\sum_\ell \ell(\ell+1)W_\ell^2 a_\ell^2\right]$$
$$\times\left[\sum_\ell(\ell-1)\ell(\ell+1)(\ell+2)W_\ell^2 a_\ell^2\right]^{-1}, \qquad (3)$$

and

$$\gamma^{*2} = \left[\sum_\ell \ell(\ell+1)W_\ell^2 a_\ell^2\right]^2\left[\sum_\ell W_\ell^2 a_\ell^2\right]^{-1}$$
$$\times\left[\sum_\ell(\ell-1)\ell(\ell+1)(\ell+2)W_\ell^2 a_\ell^2\right]^{-1}. \qquad (4)$$

Here W_ℓ are form factors taking into account beam shape and any additional smearing effect.

Assuming that signal and noise are uncorrelated, their contributions to a_ℓ^2 add up in quadrature in the (A+B) maps, $a_\ell^2 = a_{{\rm S}\ell}^2 + a_{{\rm N}\ell}^2$, and we need to determine $a_{{\rm N}\ell}^2$ in an independent way. This can be achieved by means of the (A−B) maps, which can however be used to directly derive the coefficients $A_{{\rm N}\ell}^2 = W_\ell^2 a_{{\rm N}\ell}^2$ rather than the $a_{{\rm N}\ell}^2$. Figure 2 reports the results of a harmonic best fit up to $\ell = 30$ executed on the entire celestial sphere. Increasing the number of harmonics, best fits (as well as direct integration by means of $a_{\ell m} = \int T(\theta,\phi)Y_{\ell m}^*(\theta,\phi)\mathrm{d}\Omega$) tend to overrate large-ℓ amplitudes. We checked for this effect

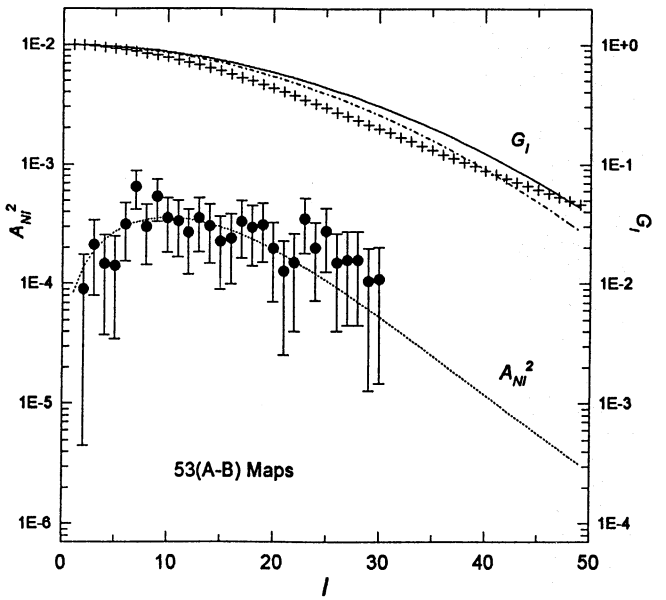

Fig. 2. The noise harmonic coefficients $A^2_{N\ell}$ (containing the form factors W^2_ℓ) and the beam shape coefficients G_ℓ vs. ℓ. Filled circles give $A^2_{N\ell}$ as obtained from the noise map, and the dotted line represents the best fit curve corresponding to $\sigma_N = 0.936°$ and $C_N = 5.74 \times 10^{-5}$ mK^2. Crosses give the experimental G_ℓ, compared to Gaussian approximations with dispersion 2.9° (full line) and 3.1° (dash-dotted)

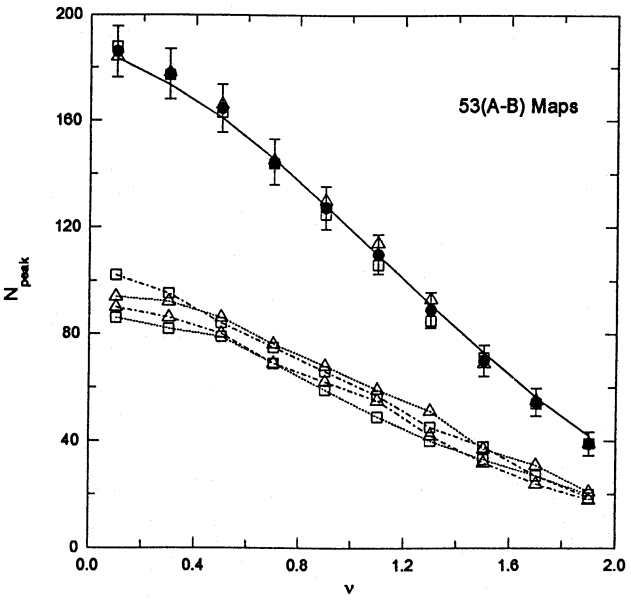

Fig. 3. The peak number N_{peak} vs. threshold in COBE-DMR noise maps. Open squares (triangles) denote positive (negative) peaks. The four lowest curves give the peak numbers extrapolated to the Northern (dotted lines) and Southern (dash-dotted) halves of the sky. The remaining curves refer to the full sky. Filled circles give the average statistics of positive and negative peaks. The full line represents the best fitting function

by considering the peak statistics for noise maps. Figure 3 gives the numbers of maxima and minima detected in the full-sky noise maps vs. threshold ν. If using Eq.s (1-4) we generate the peak statistics from a set of 50 harmonics with best-fitted amplitudes, we get a low-threshold excess of about 30 peaks with respect to the data in Fig. 2; the discrepancy increases with the number of harmonics. Since accurate theoretical calculations of peak statistics require at least ~50 harmonics, we tried to fit an analytic form to a more limited set of $A^2_{N\ell}$. A satisfactory choice is

$$A^2_{N\ell} = C_N \left(\ell + \frac{1}{2}\right) \exp\left[-\left(\ell + \frac{1}{2}\right)^2 \sigma_N^2\right]. \quad (5)$$

However the large error bars on individual $A^2_{N\ell}$ make a 2-parameter fit for the function (5) not very useful. A more convenient solution to this problem is to fit the parameter σ_N directly on the noise-generated peak distribution; using the average distribution of maxima and minima (represented by the filled circles in Figure 3) and 99 harmonics the result is $\sigma_N = 0.936° \pm 0.071°$. (We checked however that a set of $\sim 50 \div 60$ harmonics would provide a sufficient accuracy.) The fit turns out to be even "too" good, providing $\chi^2_{min} = 1.3$ against 9 degrees of freedom: This means that data points at different thresholds are not uncorrelated. The value found for σ_N is quite independent of C_N, since peak statistics does not depend on the overall amplitude of anisotropies as shown by Eq.s (3, 4).We then fitted the amplitude parameter of Eq. (5) on the reported set of $A^2_{N\ell}$ with $\ell = 2 \div 30$, getting $C_N = (5.74 \pm 0.66) \times 10^{-5}$ mK^2. The distribution described bu the full line in Fig. 3 was generated using the function (5) in the entire range $\ell = 2 \div 99$. We checked that the peak distribution of the (A-B) maps is also recovered to a good accuracy building up the harmonic spectrum with the "measured" $A^2_{N\ell}$ up to $\ell = 30$ and the function (5) at higher ℓ.

We tested power-law spectra against the peak statistics in Fig. 1 with the following procedure. For each spectrum, labelled by the spectral index n and the predicted quadrupole $Q_{rms-PS} = a_{S2}/\sqrt{4\pi}$, we generated the theoretical expectation values $a^2_{S\ell}$ and then

$$W^2_\ell a^2_\ell = G^2_\ell \exp\left[-\left(\ell + \frac{1}{2}\right)^2 \sigma_S^2\right] a^2_{S\ell} + A^2_{N\ell}. \quad (6)$$

Here G_ℓ denote the measured beam-shape coefficients of COBE-DMR. These have reported by Wright et al. (1994) up to $\ell = 50$. A more extensive set of G_ℓ up to $\ell = 99$ has been provided to us by Kogut (private communication). The exponential factor in Eq. (6) takes into account the 2.9° smearing on the map as well as the additional smearing due to orbital motion, so that our best estimate is $\sigma_S = 3.1°$. Note that σ_S should not be confused with the approximate Gaussian beamwidth which was used in many computations, but not in the present work. Also, it is quite different from the phenomenological parameter σ_N of Eq. (5). The peak distributions calculated from Eq.s (1-4) are tested against the averaged distribution of positive and negative peaks. We should notice that such theoretical distribution are affected by several sources of uncertainty. Cosmic variance

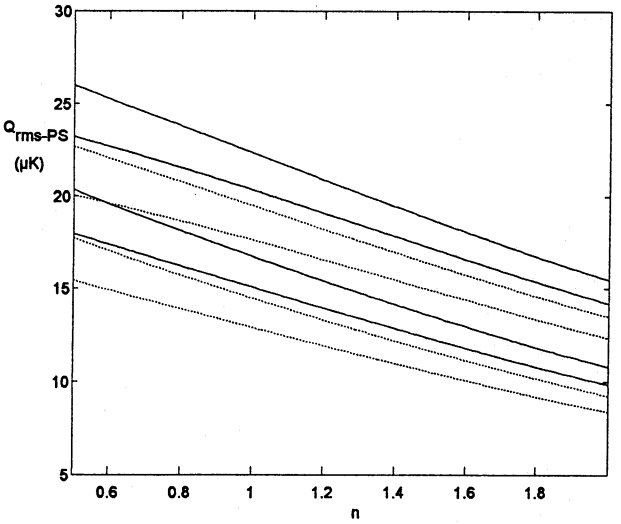

Fig. 4. The acceptance regions in the $(n, Q_{\mathrm{rms-PS}})$ plane at 1- and 2-sigma confidence levels. Contours are computed with procedures S31 (full lines) and F31 (dotted). Both procedures assume $\sigma_S = 3.1°$, $\sigma_N = 0.936°$, and $C_N = 5.74 \cdot 10^{-5}$ mK^2. The former uses the measured $A^2_{N\ell}$ up to $\ell = 30$.

(White et al. 1993) affects the cosmic-structure contribution to the harmonic coefficients $a_{\ell m}$, and a quite similar variance pertains to noise; in fact, these two effects are described by identical equations assuming that both are Gaussian processes. Performing a limited number of simulations for superpositions of Gaussian signal and noise (with fixed a^2_ℓ, the *expectation* values of harmonic strengths), we found that the probability distribution of N_{peak} at a given threshold is roughly consistent with a Poisson distribution having a width $\langle N_{\mathrm{peak}} \rangle^{\frac{1}{2}}$. However, in our case the $A^2_{N\ell}$ themselves are not fixed. When we use Eq. (5) their errors at different ℓ are correlated due to the uncertainties on C_N and σ_N; it can be shown that the corresponding contribution to the uncertainty on the predicted N_{peak} is given by

$$\mathrm{var}(N_{\mathrm{peak}}) = \left(\sum_\ell A^2_{N\ell} \frac{\partial \langle N_{\mathrm{peak}} \rangle}{\partial A^2_{N\ell}} \right)^2 \frac{\mathrm{var}(C_N)}{C_N^2}$$
$$+4 \left[\sum_\ell \left(\ell + \frac{1}{2} \right)^2 A^2_{N\ell} \frac{\partial \langle N_{\mathrm{peak}} \rangle}{\partial A^2_{N\ell}} \right]^2 \sigma_N^2 \mathrm{var}(\sigma_N). \quad (7)$$

When we use the measured $A^2_{N\ell}$, a more familiar equation $\mathrm{var}(N_{\mathrm{peak}}) = \sum_\ell \left[\left(\partial \langle N_{\mathrm{peak}} \rangle / \partial A^2_{N\ell} \right)^2 \mathrm{var}(A^2_{N\ell}) \right]$ applies. For each computed model we calculated the corresponding χ^2 combining quadratically the above errors with with the experimental error bars reported in Fig.1. This procedure allowed us to avoid a more extensive use of simulations.

Figure 4 gives the allowed regions at 1 and 2 sigmas in the $(n, Q_{\mathrm{rms-PS}})$ plane. Full lines give the contours calculated for $\sigma_S = 3.1°$, using the $A^2_{N\ell}$ of Fig. 2 up to $\ell = 30$, and the analytic form (5) with the optimal values of σ_N and C_N at higher ℓ. (This procedure is referred to as S31 in the Figure and in Table 2.) Contours calculated for $\sigma_S = 2.9°$ (case S29, not reported in the Figure) would be hardly distinguishable from them. Using the analytic form (5) in the entire range $\ell = 1 \div 99$ (case F31) the contours are slightly displaced to smaller values of $Q_{\mathrm{rms-PS}}$ (by ~ 2 μK for $n = 1$).

Table 2. Coefficients of the $n - Q_{\mathrm{rms-PS}}$ regression defined by Eq. (8)

Procedure	a (μK)	b (μK)
S31†	24.71 ± 0.65	-6.23 ± 0.45
S29 ‡	24.54 ± 0.66	-6.16 ± 0.46
F31*	21.47 ± 0.60	-5.45 ± 0.42

†$\sigma_N = 3.1°$, using noise harmonic amplitudes from Fig. (2) for $\ell \leq 30$.
‡$\sigma_N = 2.9°$
*Noise described by Eq. (5) for any ℓ

The parameters n and $Q_{\mathrm{rms-PS}}$ are clearly anticorrelated, as already found from analyses of harmonic amplitudes and the angular correlation function (Seljak & Bertschinger 1993; Torres et al. 1994; Smoot et a. 1994). Minimizing χ^2 for fixed n we identify a straight line in the $(n, Q_{\mathrm{rms-PS}})$ plane,

$$Q_{\mathrm{rms-PS}} = a + bn, \quad (8)$$

with the coefficient values listed in Table 2. From the above results, taking into account differences arising from the S31 and F31 procedures, we can conclude that $Q_{\mathrm{rms-PS}} = 17 \pm 3$ μK for $n = 1$, and $Q_{\mathrm{rms-PS}} = 14 \pm 3$ μK for $n = 1.5$. These numbers agree very well with the most likely quadrupole $Q_{\mathrm{rms-PS}}$ derived from higher order multipoles, but not with the quadrupole rms fluctuation of 6 ± 3 μK directly fitted on two-year data; see Bennet et al. (1994) for a discussion of this discrepancy, and Jing & Fang (1994) for a possible explanation in terms of an infrared cutoff in the spectrum.

Acknowledgements. We wish to thank A. Kogut for providing unpublished data on COBE-DMR beam shape. This work is partially supported by Agenzia Spaziale Italiana under Contract # 94-RS-155, by the Italian Ministry for University and Scientific and Technological Research (Progetti Nazionali e di Rilevante Interesse per la Scienza), and by the European Union under Contract # CI1*-CT92-0013.

References

Adams, F.C., et al. 1992, Phys. Rev. D47, 426
Bennett, C., et al. 1992, ApJ 396, L7
Bennett, C., et al. 1994, ApJ 436, 423
Bond, J. R., Efstathiou, G. 1987, MNRAS 226, 407
Coles, P. 1988, MNRAS 231, 125
Coles, P., Barrow, D. 1987, MNRAS 228, 407
Efstathiou, G., Bond, J.R., White, S.D.M. 1992, MNRAS 258, 1p
Fabbri, R. 1992, A&A 259, 1
Fabbri, R., Natale, V. 1993, A&A 267, L15
Fabbri, R., Natale, V. 1995, A&A 296, 289
Gorski, K.M., et al. 1994, ApJ 430, L89
Gott, J.R., et al. 1990, ApJ. 352, 1

Jing, Y.P., Fang, L.Z. 1994, Phys. Rev. Lett. 73, 1882
Kashlinsky, A. 1992, ApJ 399, L1
Kofman, L.A., Gnedin, N.Y., Bahcall, N.A. 1993, ApJ 413, 1
Martínez-González, E., Sanz, J.L. 1989, MNRAS 237, 939
Sazhin, M.V. 1985, MNRAS 216, 25p
Seljak, U., Bertschinger, E. 1993, ApJ 417, L9
Smoot, G.F., et al. 1992, ApJ 396, L1
Smoot, G.F., et al. 1994, ApJ 437, 1
Torres, S. 1994, ApJ 423, L9
Torres, S., Fabbri, R., Ruffini, R. 1994, A&A 287, 15
Vittorio, N., Juszkiewicz, R. 1987, ApJ 314, L29
White, M., Krauss, L.M., Silk, J. 1993 ApJ 418, 535
Wright, E.L., Smoot,G.F., Kogut, A., et al. 1993, ApJ 420, 1

This article was processed by the author using Springer-Verlag LaTeX
A&A style file version 3.